

Single-Crystal Dendritic Micro-Pines of Magnetic α -Fe₂O₃: Large-Scale Synthesis, Formation Mechanism, and Properties**

Minhua Cao, Tianfu Liu, Song Gao, Genban Sun, Xinglong Wu, Changwen Hu,* and Zhong Lin Wang*

Hierarchical self-assembly of nanoscale building blocks (nanoclusters, nanowires, nanobelts, and nanotubes) is a technique for building functional electronic and photonic nanodevices.^[1,2] Fractal structures are common in nature across all length scales, from self-assembled molecules, to the shapes of coastlines, to the distribution of galaxies, and even to the 3D shapes of clouds. On the nanoscale, dendritic fractals are one type of hyperbranched structure which are generally formed by hierarchical self-assembly under non-equilibrium conditions.^[3,4] Investigation of hierarchically self-assembled fractal patterns in chemical systems has shown that the distinct size, shape, and chemical functionality of such structures make them promising candidates for the design and fabrication of new functional nanomaterials,^[5] but it is challenging to develop simple and novel synthetic approaches for building hierarchically self-assembled fractal architectures of various systems.

Magnetic nanomaterials have been the subject of increasing interest due to their physical properties and technological applications.^[6-8] In the past few years, research has focused primarily on zero- and one-dimensional (1D) magnetic nanomaterials such as magnetic metals, alloys, and metal oxides and has led to substantial advances including the assembly of 2D or 3D superlattices from spherical nanoparticles or nanorods.^[9-14] However, to the best of our knowledge, the hierarchical self-assembly of magnetic nanomaterials has not been reported. Here we present the spontaneous, large-scale, hierarchical self-assembly of dendritic nanostructures of magnetic Fe₂O₃ (so-called micro-pine structure). The α -Fe₂O₃ micron-pine dendrites were synthesized by hydrothermal reaction of K₃[Fe(CN)₆] in aqueous solution at suitable temperatures. The method is based on the weak dissociation of [Fe(CN)₆]³⁻ ions under hydrothermal conditions. The resulting structures display exquisite fractal features, which morphologically resemble a type of pine tree. The structure was formed as a result of fast growth along six crystallographically equivalent directions, and this process is different from the reported formation mechanism of general fractal structures. The magnetic properties of the nanostructure show a lower Morin transition temperature of 216 K. The reported structures could have important applications in biomedical science and magnetism.

The micro-pines were synthesized on a large scale and in high purity. Figure 1 shows typical SEM images of α -Fe₂O₃

[*] Dr. M. Cao, X. Wu, Prof. C. Hu
Institute of Polyoxometalate Chemistry
Northeast Normal University
Changchun, 130024 (P. R. China)
Fax: (+86) 10-6282-8869
E-mail: huchw@nenu.edu.cn

Dr. T. Liu, G. Sun, Prof. C. Hu
The Institute for Chemical Physics
Beijing Institute of Technology
Beijing, 100081 (P. R. China)
and
Department of Chemistry
Beijing Institute of Technology
Beijing, 100081 (P. R. China)
E-mail: cwhu@bit.edu.cn

Prof. Z. L. Wang
School of Materials Science and Engineering
Georgia Institute of Technology
Atlanta, GA 30332-0245 (USA)
Fax: (+1) 404-894-8008
E-mail: zhong.wang@mse.gatech.edu

Prof. S. Gao
State Key Laboratory of Rare Earth Materials Chemistry and Applications
College of Chemistry and Molecular Engineering
Peking University
Beijing, 100871 (P. R. China)

[**] This work was supported by the Natural Science Foundation Council of China (NSFC) (No. 20271007, No. 20331010, No. 90406002, and No. 20401005), by the Specialized Research Fund for the Doctoral Program of Higher Education (SRFDP, No. 20030007014), and by Jilin Distinguished Young Scholars Program and the Natural Science Young Foundation of Northeast Normal University.

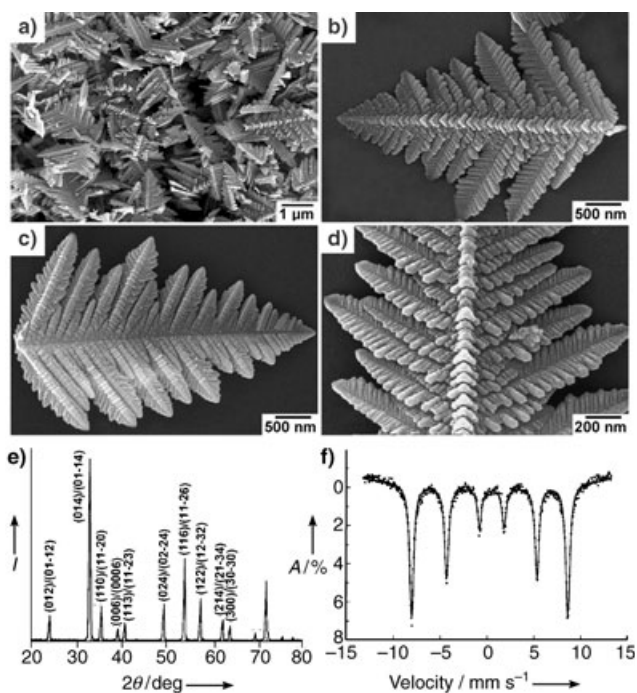


Figure 1. Electron microscopy images and chemical characterization of α -Fe₂O₃ fractals synthesized with a K₃[Fe(CN)₆] concentration of 0.015 M at 140 °C. a) Low-magnification SEM image of fractals showing the high yield and good uniformity. b) SEM image of a single α -Fe₂O₃ fractal taken from one side. c) SEM image of a single α -Fe₂O₃ fractal taken from the other side. d) A higher magnification image of a single α -Fe₂O₃ fractal showing striking periodic corrugated structures on the main trunk. e) XRD pattern of the sample confirming formation of a pure α -Fe₂O₃ phase. *I* = intensity. f) Mössbauer spectrum of the sample recorded at room temperature. *A* = absorption.

micro-pine dendrites obtained with a $\text{K}_3[\text{Fe}(\text{CN})_6]$ concentration of 0.015 M at 140 °C. The low-magnification image in Figure 1 a shows that the product consists almost entirely of such dendritic structures, and this indicates the high yield and good uniformity achieved with this approach. The high-magnification images in Figure 1 b and c show the morphology of a single dendrite in two opposite directions. They reveal a clear and well-defined dendritic fractal structure with a pronounced trunk consisting of corrugations and highly ordered branches distributed on both sides of the trunk. Figure 1 d shows striking periodic corrugated structures on the trunk of a single dendrite. The lengths of the dendrite trunks are 3–5 μm , and those of the branch trunk range from 50 nm to 1.5 μm . Note that the protrusion direction of the dendrite trunk and those of the branches are opposite, as is clearly shown by the SEM images (Figure 1 b and c), and all dendrites have similar structure. The micro-pine dendrites were shown by powder XRD (Figure 1 e) to consist of pure $\alpha\text{-Fe}_2\text{O}_3$ phase (hematite), which has a rhombohedral structure with lattice parameters of $a = 0.50355$ and $c = 1.3747$ nm. The XRD peaks are labeled by using the three- and four-index systems, as for hexagonal nanostructure. The four-index system facilitates the discussion below.

The phase composition is further supported by the room-temperature Mössbauer spectrum (Figure 1 f), which shows a single sextet with an isomeric shift of 0.44 mm s^{-1} , a quadrupole splitting of -0.23 mm s^{-1} , and a hyperfine field of 516.8 KOe and thus provides clear evidence for the presence of $\alpha\text{-Fe}_2\text{O}_3$ rather than $\gamma\text{-Fe}_2\text{O}_3$ or Fe_3O_4 .^[15] Moreover, the results of many experiments show that this approach has excellent reproducibility, and the resulting structures are highly stable, without morphological or compositional change over several months when stored in air.

The dendrite micro-pines have a single-crystalline structure. Figure 2 a shows a TEM image of a micro-pine. The TEM observations revealed that the micro-pine dendrites occasionally show a sixfold-symmetric structure (Figure 2 b), like a snowflake. Further structural characterization of the dendrite was carried out by high-resolution TEM (HRTEM). Figure 2 c–g show HRTEM images taken from the areas labeled c–g in Figure 2 a; they respectively show the lattice structures at the tip of the dendrite, the trunk of the dendrite, the tip of the dendrite branch, the trunk of the dendrite branch, and the junction between the trunk of the dendrite and that of the dendrite branch. They all show clear lattice fringes that indicate single-crystallinity of the entire dendrite structure. The lattice spacing of 2.5177 \AA between adjacent lattice planes in each of these images corresponds to the distance between two $\{11\bar{2}0\}$ crystal planes. The selected-area electron diffraction (SAED) pattern (Figure 2 g) taken from the entire dendrite clearly shows a single-crystalline structure. The diffraction pattern indicates that the dendrite is oriented along $[0001]$ with the three branches along $[10\bar{1}0]$ (or $[100]$), $[\bar{1}10]$ (or $[\bar{1}\bar{1}0]$), and $[0\bar{1}10]$ (or $[0\bar{1}0]$) (Figure 2 a). Thus, the sixfold-symmetric structure shown in Figure 2 b is a result of growth along $\pm[10\bar{1}0]$, $\pm[\bar{1}10]$, and $\pm[0\bar{1}10]$.

The reaction temperature and the concentration of $\text{K}_3[\text{Fe}(\text{CN})_6]$ significantly affect the morphology of the product. For example, when the temperature was increased from 140 to

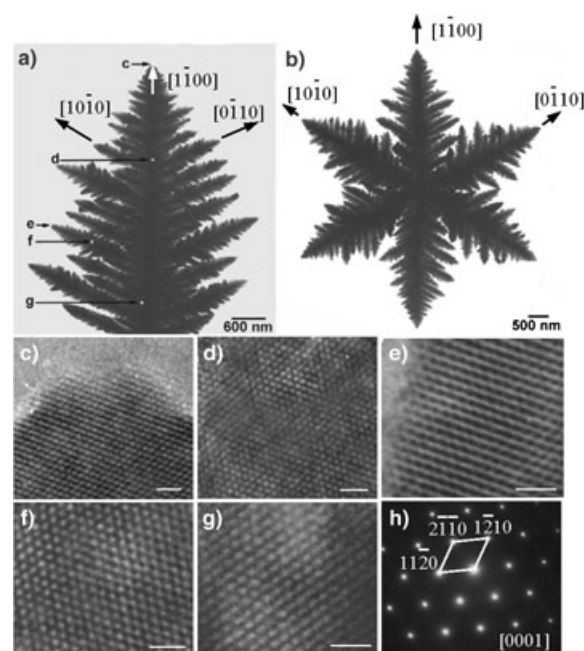


Figure 2. TEM images of the same $\alpha\text{-Fe}_2\text{O}_3$ fractals as shown in Figure 1. a) Image of a fractal exhibiting hyperbranches. b) TEM image of a sixfold-symmetric dendritic structure. c–g) High-resolution TEM images recorded in different regions of the dendritic structure in (a) showing the well-defined single-crystalline nature of the entire dendritic structure (scale bar: 1 nm). h) Electron diffraction pattern recorded from the entire dendritic structure in (a) which also shows the single-crystalline nature of the entire dendritic structure.

200 °C while keeping the concentration of $\text{K}_3[\text{Fe}(\text{CN})_6]$ constant at 0.015 M, the morphology of the sample changed continuously from hyperbranched dendrites at 140 °C (Figure 3 a) to slightly branched dendrites at 170 °C (Figure 3 b), and finally nanorod-branched dendrites at 200 °C (Figure 3 c), somewhat similar to ZnO nanowire comb structures.^[16] The

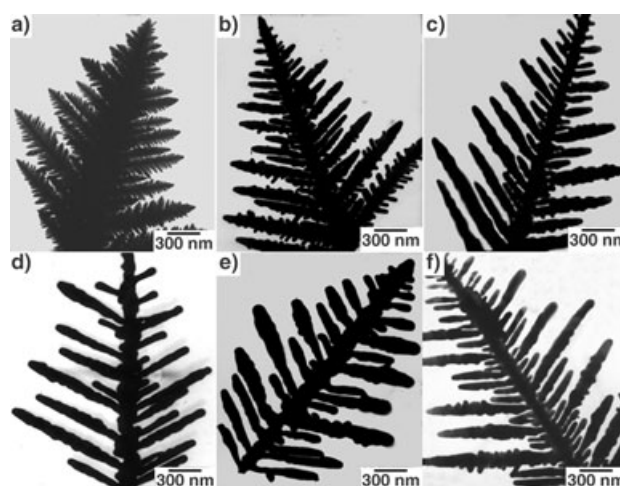


Figure 3. Evolution of crystal shape under different reaction conditions. a–c) TEM images of $\alpha\text{-Fe}_2\text{O}_3$ dendrites obtained with a concentration of $\text{K}_3[\text{Fe}(\text{CN})_6]$ of 0.01 M and reaction temperatures of 140, 170, and 200 °C, respectively. d–f) TEM images of $\alpha\text{-Fe}_2\text{O}_3$ dendrites obtained at a reaction temperature of 140 °C and concentrations of $\text{K}_3[\text{Fe}(\text{CN})_6]$ of 0.04, 0.06, and 0.1 M, respectively.

reaction temperature must be higher than 140 °C, otherwise the reaction is very slow. When the concentration of $K_3[Fe(CN)_6]$ was varied between 0.005 and 0.025 M while maintaining a constant reaction temperature of 140 °C, α - Fe_2O_3 micro-pine dendrites such as that shown in Figure 2a were the major product. However, on gradually increasing the concentration of $K_3[Fe(CN)_6]$ while maintaining the reaction temperature at 140 °C, a continuous transition from thin to thick nanorod-branched dendrites was observed. Figure 3 d–f show TEM images of samples that were synthesized at concentrations of $K_3[Fe(CN)_6]$ of 0.04, 0.06, and 0.1 M, respectively. The higher the concentration of $K_3[Fe(CN)_6]$, the thicker the nanorod branches of the dendrites. These results suggest that it is possible to control and tune the shape of α - Fe_2O_3 dendritic nanostructures by controlling the kinetic parameters of the reaction process, that is, temperature and concentration.

The formation of the dendrites could be explained by the model proposed in Figure 4. From the crystal structure, $\langle 10\bar{1}0 \rangle$ are six equivalent directions. For reasons of spatial confine-

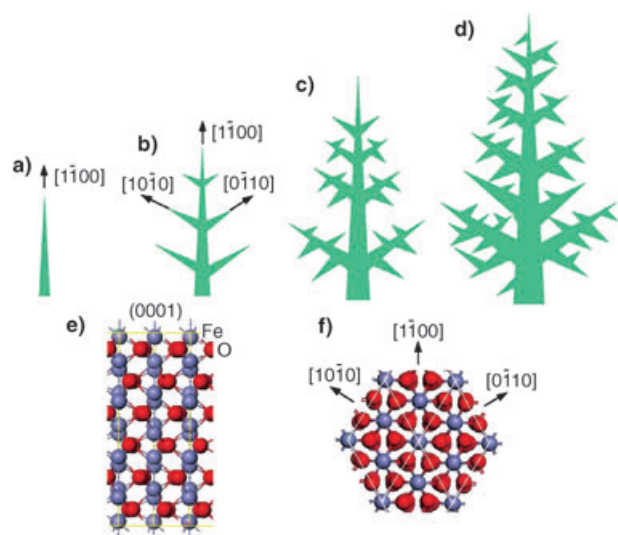


Figure 4. Proposed formation process of the micro-pine dendrite structure by fast growth along the six crystallographically equivalent directions $\langle 10\bar{1}0 \rangle$.

ment, one of the directions, for example, $[1\bar{1}00]$, initiates fast growth, and formation of a needle is possible if the growth along $[1\bar{1}00]$ is much faster than along the other directions (Figure 4a). Subsequent growth along the other two crystallographically equivalent directions, $[10\bar{1}0]$ and $[0\bar{1}10]$, leads to the formation of main and possibly symmetric branches on both sides (Figure 4b). As growth continues, each side branch can initiate growth along $\pm[0\bar{1}10]$ and $\pm[10\bar{1}0]$ to form minibranches (Figure 4c). With further growth, all of the branches become thicker and finally interconnected (Figure 4d), and form the micro-pine dendrite structure observed in Figure 1. If growth is symmetric along the six crystallographically equivalent directions $\langle 10\bar{1}0 \rangle$, a sixfold-symmetric “snowflake” structure would be formed (see Figure 2b).

To understand the reasons why the six $\langle 10\bar{1}0 \rangle$ directions are the directions of fastest growth, we start from the crystal

structure of hematite. Figure 4e shows a projection of the crystal structure along $[2\bar{1}\bar{1}0]$, which is parallel to the c plane. It is apparent that the Fe^{3+} and O^{2-} ions are arranged alternatively parallel to the c plane, which is thus terminated with either Fe^{3+} or O^{2-} and has a net ionic charge on the surface (so-called polar surface). Therefore, during synthesis in solution, the c plane will be immediately covered by adsorbing molecules to neutralize the ionic charges, which also terminate growth along $[0001]$. Therefore, the possible structure is a platelet parallel to the (0001) plane. On the other hand, the six crystallographically equivalent planes $\{2\bar{1}\bar{1}0\}/\{10\bar{1}0\}$ are neutral surfaces and are the most typical low-energy facets for a hexagonal crystal lattice (Figure 4f). Growth parallel to the c plane tends to enlarge the surfaces of $\{2\bar{1}\bar{1}0\}/\{10\bar{1}0\}$ and leads to the formation of side branches that are dominated by $\{2\bar{1}\bar{1}0\}$ and $\{10\bar{1}0\}$ surfaces.

The magnetic behavior of α - Fe_2O_3 dendritic micro-pines, which is of importance for practical applications, was investigated for the sample obtained with a $K_3[Fe(CN)_6]$ concentration of 0.015 M at 140 °C (Figure 1). The variable-temperature (5–300 K) magnetic susceptibility (Figure 5a) displays the characteristic behavior for α - Fe_2O_3 but with a lower Morin transition temperature T_M of 216 K, which is determined by the sharp peak in the $d\chi_g/dT$ curve. Normally bulk hematite has the Morin transition from the low-temperature antiferromagnetic phase to a weakly ferromagnetic phase at

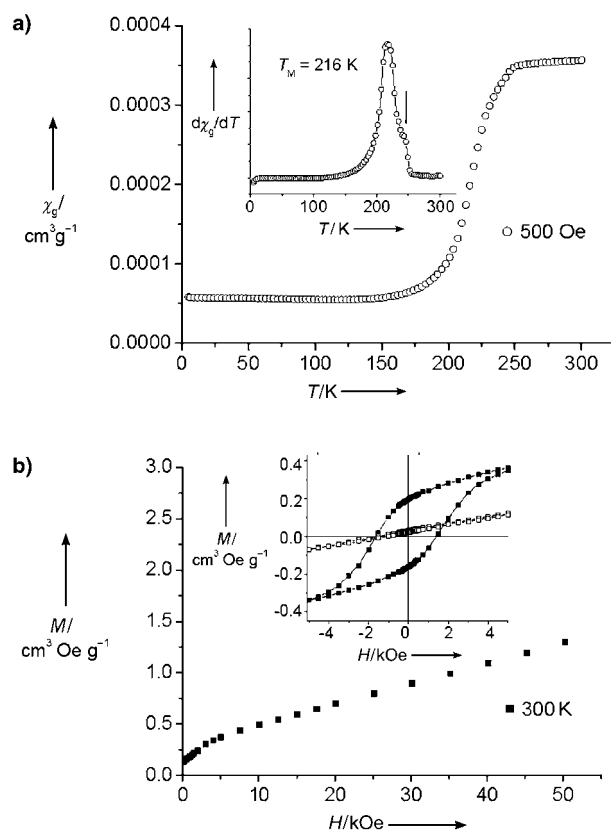
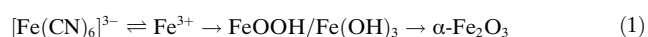


Figure 5. Magnetic measurements for the sample prepared with a $K_3[Fe(CN)_6]$ concentration of 0.015 M at 140 °C. a) Temperature dependence of magnetic susceptibility. b) Field dependence of magnetization at 5 (\square) and 300 K (\blacksquare).

260 K, and it was documented that annealing led to an increase in T_M for small-sized hematite.^[17] The decrease in T_M here may result from some lattice strain and defects in the dendrites obtained by low-temperature hydrothermal synthesis. Superparamagnetic phenomena were not found for the sample, since the sizes of the branch trunk are rather large (50 nm to 1.5 μm) compared to the single-domain size of hematite. The shoulder around 243 K in the $d\chi_g/dT$ curve may indicate the presence of a larger trunk with higher T_M . The field dependence of the magnetization at 300 and 5 K (Figure 5b) confirm the antiferromagnetic state at low temperature and weak ferromagnetism above T_M . The coercive force at 300 K of 1510 Oe is larger than that of 1080 Oe for spherical hematite with a diameter of 160 nm, which might be due to the shape anisotropy of the dendrites.^[17]

We recently employed a soft-templating route for fabricating well-crystallized 1D nanostructures based on self-assembly of surfactants and inorganic precursors.^[18–20] However, the disadvantage of this method is that the presence of the surfactants can easily result in the formation of byproducts, which may limit their applications. In the present study, we emphasize the role of the $\text{K}_3[\text{Fe}(\text{CN})_6]$ complex as a single precursor in the synthesis of nanomaterials. $\text{K}_3[\text{Fe}(\text{CN})_6]$ plays a crucial role in the formation of dendritic fractal structures; if other iron sources such as FeCl_3 , $\text{Fe}(\text{NO}_3)_3$, and $\text{Fe}_2(\text{SO}_4)_3$, are used, even under the same reaction conditions, only particles are observed instead of micro-pine dendrites. $[\text{Fe}(\text{CN})_6]^{3-}$ ions are very stable ($K_s = 1.0 \times 10^{42}$) in aqueous solution at room temperature, and almost no free Fe^{3+} ions can be detected. However, in our case, we believe that $\alpha\text{-Fe}_2\text{O}_3$ formation proceeds through three steps [Eq. (1)] under the hydrothermal conditions: first, $[\text{Fe}(\text{CN})_6]^{3-}$ ions dissociate slowly into Fe^{3+} ions; second, the Fe^{3+} ions are subsequently hydrolyzed in aqueous solution to form FeOOH or $\text{Fe}(\text{OH})_3$; and finally, the resulting FeOOH or $\text{Fe}(\text{OH})_3$ decompose into $\alpha\text{-Fe}_2\text{O}_3$. This growth process might be determined by the first step because of the weak dissociation tendency of $[\text{Fe}(\text{CN})_6]^{3-}$ ions [Eq. (1)].



Dendritic fractals of several materials have been found and investigated.^[21–27] It is generally accepted that fractal aggregation arises in situations far from thermodynamic equilibrium where high driving forces lead to the generation of rough crystallites and random association.^[24] In the past few years the model known as diffusion-limited aggregation (DLA) has been successfully developed to interpret this ramified growth of different systems controlled by diffusive processes.^[28] In our system, the formation of micro-pine dendrites of $\alpha\text{-Fe}_2\text{O}_3$ is a new growth process in which fast growth along six crystallographically equivalent directions forms single-crystal dendrites or snowflakelike structures.

We have described a distinct type of hierarchical $\alpha\text{-Fe}_2\text{O}_3$ micro-pine dendrite. Formation of such structures requires a suitable iron complex precursor that slowly dissociates to yield Fe^{3+} ions under the hydrothermal conditions. Our experimental method also provides a simple and facile route

for the preparation of $\alpha\text{-Fe}_2\text{O}_3$ nanostructures, which could have important applications in biomedical science due to the biodegradability of iron oxide. It could also be a general approach for the large-scale, high-purity growth of dendritic fractal structures of a wide range of materials.

Experimental Section

$\alpha\text{-Fe}_2\text{O}_3$ micro-pine dendrites were synthesized by hydrothermal reaction of $\text{K}_3[\text{Fe}(\text{CN})_6]$ in aqueous solutions at suitable temperatures. In a typical synthesis, $\text{K}_3[\text{Fe}(\text{CN})_6]$ was dissolved in distilled water to form a clear solution of a certain concentration, which was placed in a Teflon-sealed autoclave and maintained at a given temperature for 2 d. The red product was isolated by centrifugation, repeatedly washed with distilled water and absolute ethanol, and dried at 50 °C in air. The concentration of $\text{K}_3[\text{Fe}(\text{CN})_6]$ was varied in the range from 0.005 to 0.1 M, and the reaction temperature from 140 to 200 °C.

X-ray diffraction (XRD) was performed on a Japan Rigaku D/max γA X-ray diffractometer with graphite-monochromatized $\text{Cu}_{\text{K}\alpha}$ radiation ($\lambda = 0.154178$ nm). A JEOL JEM-2010F transmission electron microscope operating at 200 kV accelerating voltage was used for TEM (transmission electron microscopy) analysis. Scanning electron microscopy (SEM) was performed with an Amray 1910FE microscope. The Mössbauer spectrum was recorded on a conventional Mössbauer spectrometer with a room-temperature ^{57}Co source (Rh matrix) in transmission geometry. Magnetic measurements were performed on a Quantum Design MPMS-XL5 SQUID magnetometer.

Received: February 6, 2005

Published online: ■ ■ ■ ■ ■, 2005

Keywords: fractals · hydrothermal synthesis · iron oxides · magnetic properties · nanostructures

- [1] R. L. Whetten, J. T. Khoury, M. M. Alvarez, S. Murthy, I. Vezmar, Z. L. Wang, C. C. Cleveland, W. D. Luedtke, U. Landman, *Adv. Mater.* **1996**, *8*, 428.
- [2] S. Sun, C. B. Murray, D. Weller, L. Folks, A. Moser, *Science* **2000**, *287*, 1989.
- [3] a) I. Lisiecki, P. A. Albouy, M. P. Pileni, *Adv. Mater.* **2003**, *15*, 712; b) T. A. Witten, Jr., L. M. Sander, *Phys. Rev. Lett.* **1981**, *47*, 351.
- [4] P. Meakin, *Phys. Rev. Lett.* **1983**, *51*, 1119.
- [5] P. D. Yang, T. Deng, D. Y. Zhao, P. Y. Feng, D. Pine, B. F. Chmelka, G. M. Whitesides, G. D. Stucky, *Science* **1998**, *282*, 2244.
- [6] D. Zitoun, M. Respaud, M. C. Fromen, M. J. Casanove, P. Lecante, C. Amiens, B. Chaudret, *Phys. Rev. Lett.* **2002**, *89*, 37203.
- [7] X. G. Wen, S. H. Wang, Y. Ding, Z. L. Wang, S. H. Yang, *J. Phys. Chem. B* **2005**, *109*, 215.
- [8] E. V. Shevchenko, D. V. Talapin, H. Schnablegger, A. Kornowski, O. Festin, P. Svedlindh, M. Haase, H. Weller, *J. Am. Chem. Soc.* **2003**, *125*, 9090.
- [9] a) L. Q. Xu, W. Q. Zhang, Y. W. Ding, Y. Y. Peng, S. Y. Zhang, W. C. Yu, Y. T. Qian, *J. Phys. Chem. B* **2004**, *108*, 10859; b) S. J. Park, S. Kim, S. Lee, Z. G. Khim, K. Char, T. Hyeon, *J. Am. Chem. Soc.* **2000**, *122*, 8581.
- [10] a) V. F. Puentes, K. M. Krishan, A. P. Alivisatos, *Science* **2001**, *291*, 2115; b) V. F. Puentes, D. Zanchet, C. K. Erdonmez, A. P. Alivisatos, *J. Am. Chem. Soc.* **2002**, *124*, 12874.

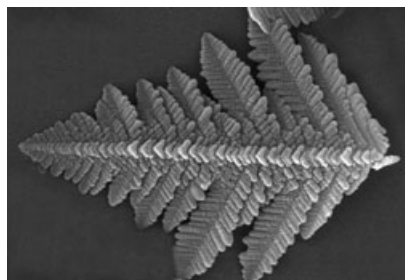
- [11] a) F. Dumestre, B. Chaudret, C. Amiens, M. Respaud, P. Fejes, P. Renaud, P. Zurcher, *Angew. Chem.* **2003**, *115*, 5371; *Angew. Chem. Int. Ed.* **2003**, *42*, 5213; b) F. Dumestre, B. Chaudret, C. Amiens, M. C. Fromen, M. J. Casanove, M. Respaud, P. Zurcher, *Angew. Chem.* **2002**, *114*, 4462; *Angew. Chem. Int. Ed.* **2002**, *41*, 4286.
- [12] N. Cordente, M. Respaud, F. Senocq, M. J. Casanove, C. Amiens, B. Chaudret, *Nano Lett.* **2001**, *1*, 565.
- [13] J. Park, B. Koo, Y. Hwang, C. Bae, K. An, J. G. Park, H. M. Park, T. Hyeon, *Angew. Chem.* **2004**, *116*, 2332; *Angew. Chem. Int. Ed.* **2004**, *43*, 2282.
- [14] a) E. V. Shevchenko, D. V. Talapin, A. L. Rogach, A. Kornowski, M. Haase, H. Weller, *J. Am. Chem. Soc.* **2002**, *124*, 11480; b) E. V. Shevchenko, D. V. Talapin, H. Schnablegger, A. Kornowski, O. Festin, P. Svedlindh, M. Haase, H. Weller, *J. Am. Chem. Soc.* **2003**, *125*, 9090.
- [15] R. M. Cornell, U. Schwertmann, *The Iron Oxides*, VCH, Weinheim, **1996**.
- [16] Z. L. Wang, X. Y. Kong, J. M. Zuo, *Phys. Rev. Lett.* **2003**, *91*, 185502.
- [17] T. P. Raming, A. J. A. Winnubst, A. C. M. van Kats, A. P. Philipse, *J. Colloid Interface Sci.* **2002**, *249*, 346.
- [18] a) M. H. Cao, C. W. Hu, G. Peng, Y. J. Qi, E. B. Wang, *J. Am. Chem. Soc.* **2003**, *125*, 4982; b) M. H. Cao, C. W. Hu, E. B. Wang, *J. Am. Chem. Soc.* **2003**, *125*, 11196.
- [19] M. H. Cao, Y. H. Wang, C. X. Guo, Y. J. Qi, C. W. Hu, *Langmuir* **2004**, *20*, 4784.
- [20] a) M. H. Cao, C. W. Hu, Y. H. Wang, Y. H. Guo, C. X. Guo, E. B. Wang, *Chem. Commun.* **2003**, 1884; b) G. B. Sun, M. H. Cao, Y. H. Wang, C. W. Hu, L. Ren, K. L. Huang, *Chem. Commun.* **2005**, 1740.
- [21] a) S. T. Selvan, *Chem. Commun.* **1998**, 351; b) X. Q. Wang, K. Naka, H. Itoh, S. Park, Y. Chujo, *Chem. Commun.* **2002**, 1300.
- [22] a) J. P. Xiao, Y. Xie, R. Tang, M. Chen, X. B. Tian, *Adv. Mater.* **2001**, *13*, 1887; b) Y. Zhou, S. H. Yu, C. Y. Wang, X. G. Li, Y. R. Zhu, Z. Y. Chen, *Adv. Mater.* **1999**, *11*, 850.
- [23] M. Wang, S. Zhong, X. B. Yin, J. M. Zhu, R. W. Peng, Y. Wang, K. Q. Zhang, N. B. Ming, *Phys. Rev. Lett.* **2001**, *86*, 3827.
- [24] M. Wang, X. Y. Liu, C. S. Strom, P. Bennema, W. Enckevort, N. B. Ming, *Phys. Rev. Lett.* **1998**, *80*, 3089.
- [25] J. Zhu, S. Liu, O. Palchik, Y. Koltypin, A. Gedanken, *Langmuir* **2000**, *16*, 6396.
- [26] a) Z. G. R. Tian, J. Liu, J. A. Voigt, H. F. Xu, M. J. Mcdermott, *Nano Lett.* **2003**, *3*, 89; b) A. Parfenov, I. Gryczynski, J. Malicka, C. D. Geddes, J. R. Lakowicz, *J. Phys. Chem. B* **2003**, *107*, 8829.
- [27] Q. Peng, Y. J. Dong, Z. X. Deng, Y. D. Li, *Inorg. Chem.* **2002**, *41*, 5249.
- [28] a) R. R. Brady, R. C. Ball, *Nature* **1984**, *309*, 225; b) M. Wang, N. B. Ming, *J. Phys. Chem. B* **1993**, *48*, 3825.

Communications

Fractal Iron Oxide

M. Cao, T. Liu, S. Gao, G. Sun, X. Wu,
C. Hu,* Z. L. Wang* — 2289–2296

Single-Crystal Dendritic Micro-Pines of
Magnetic α -Fe₂O₃: Large-Scale Synthesis,
Formation Mechanism, and Properties



Fractal hematite dendrites with structures resembling pine trees (see picture) were obtained by hydrothermal treatment of K₃[Fe(CN)₆]. They are formed by a novel process in which fast growth along six crystallographically equivalent directions forms dendritic or snowflakelike single-crystal structures, which differs from the mechanisms reported for other fractal structures.